

X-ray Measurement of the subpixel structure of the XMM EPIC MOS CCD

H. TSUNEMI ^{a,b}, K. YOSHITA ^a, A.D. SHORT ^c, P. J. BENNIE ^c,
M.J.L. TURNER ^c, A. F. ABBEY ^c

^aDepartment of Earth and Space Science, Graduate School of Science, Osaka University,
1-1 Machikaneyama-cho, Toyonaka, Osaka 560-0043, Japan

^bCREST, Japan Science and Technology Corporation (JST)

^cX-ray Astronomy Group, Department of Physics & Astronomy, Leicester University

Accepted in Nucl. Instr. and Methods A, 1999

ABSTRACT

We report here the results of a mesh experiment to measure the subpixel structure of the EPIC MOS CCDs on board the XMM X-ray observatory. The pixel size is $40\ \mu\text{m}$ square while the mesh hole spacing is $48\ \mu\text{m}$, a combination quite different from our standard mesh experiment. We have verified that this combination functions properly and have analyzed the CCD structure with sub-pixel resolution.

The EPIC MOS CCD has an open electrode structure to improve detection efficiency at low energies. We obtained the distribution of various grades of X-ray events inside the pixel. A horizontally split two-pixel event is generated near the channel stop which forms a straight vertical pixel boundary whereas a vertically split two-pixel event is generated where the potential due to the thinned gate structure forms a wavy horizontal pixel boundary. Therefore, the effective pixel shape is not a square but is distorted.

The distribution of X-ray events clearly shows that the two etched regions in each pixel, separated by the bridging finger of the enlarged (open) electrode. We measured the difference in X-ray transmission between the conventional and open regions of the pixel using O-K and Cu-L X-ray emission lines, and found it to be consistent with an electrode thickness comprising $0.2 \pm 0.1\ \mu\text{m}$ of *Si* and $0.6 \pm 0.2\ \mu\text{m}$ of *SiO₂*.

KEY WORDS: charge-coupled-device, mesh experiment, open electrode, subpixel resolution

1. Introduction

The Charge-Coupled Device (CCD) is now widely used in X-ray photon counting detector applications, and particularly in X-ray astronomy [1]. CCDs consist of many small pixels each of which functions as an independent detector. When an X-ray photon is absorbed in a CCD, it produces a finite charge cloud. When the photo-absorption occurs in the depletion layer, the entire charge cloud is collected and read out as a signal, but a total charge is often shared between several adjacent pixels each of which has a signal greater than the detection threshold. In this way X-ray events fall into different grades; single-pixel events, vertically split two-

pixel events, horizontally split two-pixel events, 3–4 pixel split events etc. The type of event observed depends principally upon the proximity of the X-ray's absorption to a pixel boundary, as well as on its energy and its depth. In this sense it is the real pixel boundary as defined by the potentials within the device, and not simply the geometrical arrangement of electrodes which is important. The total charge (proportional to the X-ray energy) can be measured by summing the signals from all pixels associated with the event.

The response function of a CCD can be divided into three parts: the gate structure transmission, the absorption efficiency in the deple-

tion region, and the charge spreading after the photo-electric absorption. We usually calibrate CCDs by uniformly irradiating them with X-rays at a number of discrete energies. In this way, X-rays are incident with equal probability upon all regions of the pixel, and the calibration data contain effects which cannot be measured separately. However, since the thickness of the gate and the depletion region vary within each pixel, the detection efficiency must also vary. To obtain a realistic response function of the CCD for the data analysis, it is therefore necessary to extract the response from different regions within the pixel.

Recently, a new technique has been introduced to obtain the X-ray response of the CCD with sub-pixel resolution [2]. The technique consists of a metal mesh positioned just above the CCD and a parallel beam of X-rays. The holes in the mesh are smaller than the CCD pixel size and have periodic spacing. This technique enables us to restrict the incident X-ray position with sub-pixel resolution. The sub-pixel structures of the various types of the CCD (ASCA SIS, AXAF ACIS etc.) have been measured using this mesh technique [3, 4]. In this paper, we report on a measurement of the EPIC MOS (Metal Oxide Semiconductor) ‘open electrode’ CCD developed for the XMM observatory.

2. EPIC MOS CCDs

The EPIC cameras [5] are focal plane imaging spectrometers developed for XMM [6]. There are three cameras, situated at the foci of the three mirror modules, and all carry silicon CCD detectors. One of the cameras utilizes PN technology CCDs and has been developed by the Max Planck Institute. The other two cameras carry MOS CCDs (EEV CCD22) and have been developed by the X-ray Astronomy Group at Leicester University [7]. The EEV CCD22 is a frame transfer, front-illuminated device. The image section consists of a 600×600 arrays of $40 \mu\text{m}$ square pixel.

The CCD22 is a three phase device, and the electrodes, or gates (poly 1, 2 and 3) are shown

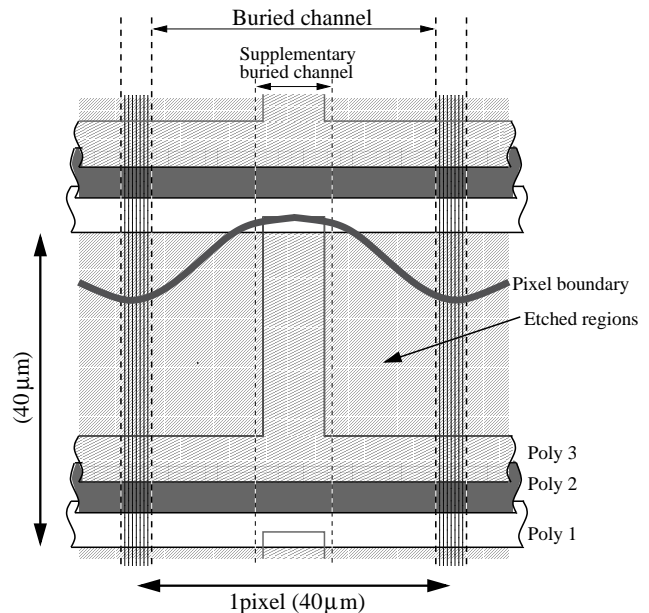


Fig. 1. Schematic view of the gate structure [7] of the CCD we employed. There are three gates: one of them is partly thinned in order to improve the detection efficiency at low energy. The wavy line denotes the horizontal pixel boundary.

schematically in Fig. 1 [7]. In order to obtain a useful X-ray detection efficiency at low energies, one of the gates, poly-3, has been enlarged and two holes have been left, through this enlarged gate to the native oxide layer. These two holes are separated by a central electrode ‘finger’. A P^+ dopant is implanted in the etched areas, which pins the surface potential to the substrate potential.

3. Experimental Setup

The experiment was performed in a CCD test facility at Leicester University. The principle of the mesh experiment is described in Tsunemi *et al.* [2] There are normally two types of mesh experiment: a single-pitch mesh experiment and a multi-pitch mesh experiment [8]. In the single-pitch mesh experiment, we employ a mesh whose hole spacing is equal to that of the CCD pixel size, while in the multi-pitch mesh experiment, we employ a mesh whose hole spacing is a multiple of the CCD pixel size. For this experiment we employed a copper mesh with a thickness of

10 μm . It has holes of 3.4 μm diameter, periodically spaced at 48 μm intervals. This mesh was originally designed in order to perform the multi-pitch mesh experiment using CCDs with 12 μm square pixels [9]. A novel feature of this experiment was therefore that the mesh hole spacing is not an integer multiple of the CCD pixel size. This makes the analysis slightly more complicated. The mesh was placed approximately 2 mm above the CCD and was rotated slightly with respect to the CCD edges.

The X-ray source was approximately 3 m from the CCD and several fluorescence targets were used, generating characteristic X-rays as well as a bremsstrahlung spectrum. We mainly selected the emission lines for analysis. Figure 2 shows a typical X-ray spectrum obtained by selecting only single-pixel events. It includes emission lines of O-K (0.52 keV), Cu-L (0.93 keV) and Si-K (1.74 keV). The energy range below 0.3 keV is enhanced by C-K (0.28 keV). In our experiment, we only used the O-K and Cu-L emission lines and we placed a pinhole of 5 mm diameter in front of the X-ray generator to restrict the beam divergence, but the effective mesh hole shadow on the CCD was still estimated to be about 7 μm . The X-ray generator current was restricted so that X-ray photons did not heavily pile up on the CCD.

The CCD operating conditions were identical to those employed on the XMM satellite. The chip was cooled to -100°C using liquid nitrogen and was driven using duplicate flight electronics.

4. Mesh experiment

In the mesh experiment, the incident X-ray position on the CCD is restricted by the mesh hole size which is smaller than the CCD pixel size. Equation (1) shows the relation between the CCD coordinate, \mathbf{X} , and the mesh coordinate, \mathbf{x} .

$$\begin{aligned} \mathbf{X} &= M\mathbf{x} + \mathbf{X}_{\text{off}} \\ &= m \begin{pmatrix} 1+a & 0 \\ 0 & 1+b \end{pmatrix} \begin{pmatrix} \cos\theta & -\sin\theta \\ \sin\theta & \cos\theta \end{pmatrix} \mathbf{x} \\ &\quad + \mathbf{X}_{\text{off}} \end{aligned} \quad (1)$$

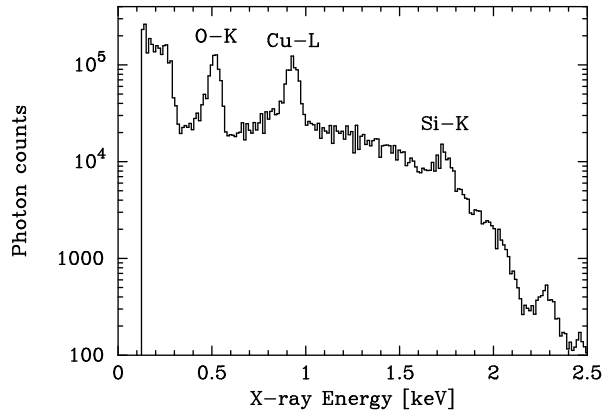


Fig. 2. X-ray spectrum obtained with single-pixel events. There are three characteristic X-ray emissions: O-K, Cu-L and Si-K. We employed O-K and Cu-L for the analysis.

where m is the mesh experiment multiplier, a and b are expansion coefficients along the x and y axes, θ is the tilt angle and \mathbf{X}_{off} is an offset.

Therefore, in order to reconstruct the sub-pixel response of the CCD, it is first necessary to determine these parameters for the experimental alignment between the mesh and the CCD with sub-pixel precision. The standard mesh experiment is performed with m an integer [2, 3, 4, 8, 9] and the raw data clearly shows a moire pattern from which approximate values for the parameters may be calculated. Then we can easily determine the mutual alignment between the mesh and the CCD with sufficient precision to reconstruct the sub-pixel response. The detailed data reduction method is described in [8, 10].

In this experiment, m has a non-integer value of 1.2. Figure 3 shows a raw image of Cu-L single-pixel events. The intensity is not uniform, but shows a resonance between the CCD pixel size and the mesh hole spacing. Assuming that single-pixel events occur when X-rays are incident upon the inner part of the pixel, we calculate a parameter $Dist$, the distance between a pixel giving single-pixel events and its nearest associated hole position. This parameter is defined in eq.(2)[12].

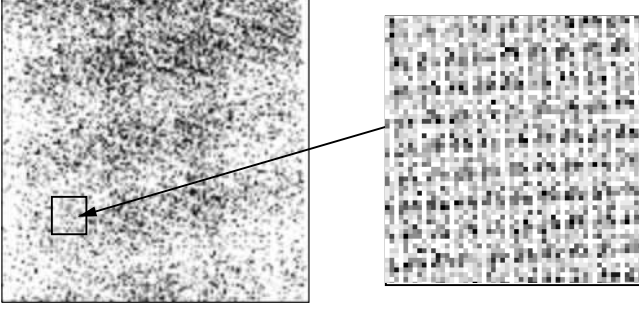


Fig. 3. Raw image of single-pixel events shows a moiré pattern. We see a periodic structure generated by the resonance between the CCD pixel spacing and the mesh hole spacing.

$$Dist(a, b, \theta, \mathbf{X}_{\text{off}}) = \sum_i^{\text{pixel}} (\mathbf{X}_{\text{hole}} - \mathbf{X}_i)^2 N_i, \quad (2)$$

$$\mathbf{X}_{\text{hole}} = M \mathbf{x}_{\text{hole}} + \mathbf{X}_{\text{off}}$$

where \mathbf{X}_i is the position of the CCD of the i th pixel, N_i is the number of single-pixel events detected in the i th pixel, and \mathbf{x}_{hole} is the hole position nearest to the i th pixel. $Dist$ is a function of a, b, θ and \mathbf{X}_{off} and the true values of these parameters may be found by minimizing $Dist$. In this way, we determined the best fit values as $a = 0.8 \times 10^{-3}$, $b = 0.9 \times 10^{-3}$, $\theta = 0.09^\circ$ and $\mathbf{X}_{\text{off}} = (0.81, 0.33)$.

5. Restored Image

In the mesh experiment, there are two ways to restore the image: one is restoration onto the CCD coordinate system, and the other is restoration onto the mesh coordinate system [10]. In this, non-standard experiment, we restored the image onto the mesh coordinate system. The restored image is a ‘representative unit’ (RU) of $48 \mu\text{m}$ square which is a convolution of the effective holes and the CCD pixel structure ($40 \mu\text{m}$ square).

Figure 4 shows examples of 2×2 RUs for various event grades. We set the split threshold level to be 63 eV throughout our analysis. The RU for single-pixel events has four isolated parts. In the RU for vertically split two-pixel events, we clearly see four wavy structures near the top and

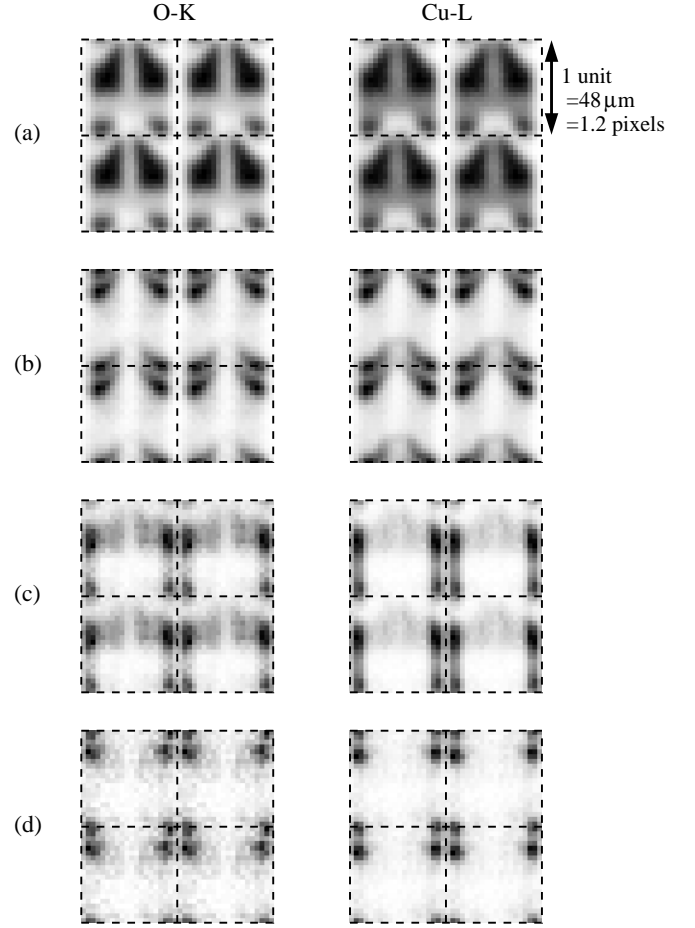


Fig. 4. 2×2 representative units (on the mesh coordinate) for (a) single-pixel events, (b) vertically split two-pixel events, (c) horizontally split two-pixel events and (d) corner events. Restored images for O-K are in the left column while those for Cu-L are in the right column.

bottom of each pixel. The structures near the top correspond to two-pixel split events in which the greater charge is in the lower pixel, while those near the bottom corresponds to two-pixel split events in which the greater charge is in the upper pixel. Therefore, the gap between these regions, corresponds to the pixel boundary. We should note that the horizontal pixel boundary is not a straight line but is curved. However, the pixel boundary in the vertical direction is a straight line which is seen in the RU for horizontally split two-pixel events. The 3–4 pixel split events appear near the pixel corners as one would expect.

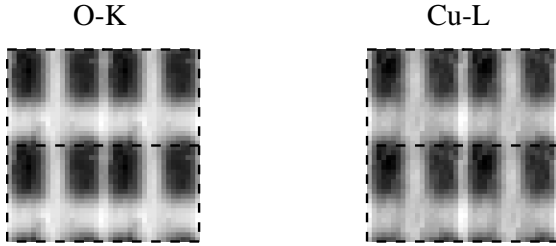


Fig. 5. 2×2 representative pixel (on the CCD coordinate) arrays for all events. Dashed lines represent the $40 \mu\text{m}$ square array.

A pixel boundary is a region where the electric potential forms a barrier to electrons during integration. The vertical boundaries are formed by the channel stops, and the gates form the horizontal boundaries. The poly-3 gate has been partially removed in order to increase the low energy detection efficiency, leaving a central finger in order to transfer the charge to the adjacent pixel. The schematic view in Fig. 1 shows the predicted horizontal pixel boundary as a thick, wavy line. The pixel boundaries in conventional CCD chips are straight lines in both the horizontal and vertical directions, the wavy boundary being a feature of the ‘open’ gate structure.

We reconstructed the CCD pixel image using all X-ray events, taking into account the wavy boundary. The reconstructed image is a ‘representative pixel’ (RP) of $40 \mu\text{m}$ square. Figure 5 shows the CCD responsivity of 2×2 RPs. We clearly see that there are two regions in the pixel where the X-ray responsivity is enhanced particularly for low energy X-rays. These enhanced regions coincide with the open sections of the pixel.

Due to the relatively large effective diameter of the mesh holes, it was not possible to accurately measure the shape of the thinned gate area during this experiment. From other experiments, scanning electron microscope (SEM) images, and information gained during device fabrication however, the open area is known to be about 40% of the total pixel area. Therefore, we simply assumed that 40% of each pixel has an enhanced responsivity while the remainder is covered by a uniform conventional gate struc-

ture. This assumption does not realistically represent the gate overlaps, the difference in thickness between the different gates or the channel stops. These fine structures will be studied in detail in the next experiment, which will utilize a mesh with a much finer effective mesh hole size.

Based on our simple assumption, we measured the difference in the electrode absorption between the thinned gate region and the rest of the pixel, in terms of an effective absorber thickness. For this we used O-K and Cu-L data for which we had sufficient statistics. Since these two lines are respectively below and above the O-K edge, we are able to determine the differences in thickness between the thinned gate area and the rest of the pixel, for *Si* and *SiO₂* independently. They are $0.2 \pm 0.1 \mu\text{m}$ for *Si* and $0.6 \pm 0.2 \mu\text{m}$ for *SiO₂*. We should note that the errors in these two results are strongly correlated with each other.

6. Discussion

X-rays detected by a photon counting CCD form events which fall into several grades (single-pixel, two-pixel etc.). The grade of event depends principally upon the position within the CCD pixel at which the X-ray photon is absorbed. The pixel boundaries of conventional CCDs form a simple square [2, 3, 4, 9, 12], the vertical pixel boundary being formed by the channel stops which are straight lines, and the horizontal pixel boundaries being formed by clocking gates which are also straight lines.

The EEV CCD22, having an open electrode structure, exhibits quite different boundaries. The vertical pixel boundary is still a straight line since the channel stops are straight, but the horizontal pixel boundaries are wavy due to the open gate structure. This is because the potential in some parts of the open region is determined by the electrode of the neighboring pixel, so that the potential barrier separating the pixels is located within the open area and not under the electrodes.

Since the horizontal pixel boundary runs

Table 1. Branching ratio of the X-ray event grades

	O-K	Cu-L
Energy (keV)	0.52	0.93
Single-pixel (%)	81.3	79.0
Vertically split two-pixel (%)	15.3	16.2
Horizontally split two-pixel (%)	3.0	4.0
3-4 pixel (%)	0.4	0.8

through the open electrode region, some of the X-ray photons incident upon this open region form charge clouds which are collected in the neighboring pixel, and others give rise to vertically split two-pixel events rather than single-pixel events as seen in Figure 4. Since the X-ray photon energy is measured by summing the charge from all pixels comprising the event, a single-pixel event usually shows better energy resolution than split-pixel events. Table 1 shows the branching ratio i.e. the fraction of X-ray events forming each grade of events. These values are obtained by eliminating the pile-up effects.

We also observe that vertically split two-pixel events are detected with a greater efficiency than horizontally split two-pixel events. This is consistent with them being generated in the open region rather than under the electrodes. The ratio between the horizontally split two-pixel events and the vertically split two-pixel events depends partly on the charge cloud shape and size, and has previously been used as a diagnostic [9, 11, 13]. However, in this case, the difference in detection efficiency for the two grades of event significantly alters the branching ratio, making it difficult to evaluate the charge cloud shape.

We restored the CCD pixel image using all the X-ray events and found that there are two regions in each pixel where the detection efficiency is enhanced. There are four regions where single-pixel events are generated, two of which are separated by the regions where the vertically split two-pixel events are generated. These regions are located in the open electrode area, and this is confirmed by increased detection efficiency.

The XMM MOS CCD has a relatively large

pixel size ($40\ \mu\text{m}$ square). This is significantly larger than other devices to which this technique has been applied including the ASCA SIS [3] ($27\ \mu\text{m}$) and AXAF ACIS [4] ($24\ \mu\text{m}$). However, the majority of the pixel is occupied by the third phase, much of which is open (i.e. is not covered by polysilicon electrode) in order to increase the detection efficiency at low energies. The scale of the gate structures and overlaps themselves are of the order of one μm . In order to obtain the precise response function of the CCD in future experiments it will therefore be necessary to use a mesh with a smaller hole size and a less divergent X-ray beam.

7. Conclusion

We performed a mesh experiment using a CCD with an open gate structure developed for the XMM satellite. The mesh hole spacing was 1.2 times greater than the CCD pixel spacing which is a different configuration from the standard mesh experiment. We confirmed that this configuration functions properly although a completely different moire pattern results. We employed a distance measure to determine the parameter values for the mesh experiment. In this way, we have succeeded in restoring an image with which we can see where the X-rays are absorbed within the CCD pixel.

The distribution of the various X-ray event grades are quite different from those obtained using more conventional CCDs. The vertical pixel boundary is represented by a straight line which is formed by the channel stop. However, the horizontal pixel boundary is represented by a wavy line between the poly-1 and the poly-3 electrodes. The horizontally split two-pixel events are generated in the region near the channel stop whereas the vertically split two-pixel events are generated in the open electrode region where the detection efficiency is enhanced. The effective pixel shape is not a $40\ \mu\text{m}$ square but a distorted shape with an area equal to a $40\ \mu\text{m}$ square.

Vertically split two-pixel events are much more numerous than horizontally split two-pixel

events, particularly at low energies. We confirmed that this is because they are formed by X-ray absorption in the open gate region where the detection efficiency is greatly enhanced. By comparing the detection efficiency from the open part of the pixel with an average value for the rest of the pixel, an equivalent absorber thickness of $0.2 \pm 0.1 \mu\text{m}$ for *Si* and $0.6 \pm 0.2 \mu\text{m}$ for *SiO₂*. In order to better resolve the pixel structure for the CCD data analysis, the next experiment will utilize a mesh with smaller holes and a less divergent X-ray beam.

8. Acknowledgements

We wish to express our thanks to all the member of the X-ray Astronomy Group in Leicester University for their assistance and comment. KY is partly supported by JSPS Research Fellowship for Young Scientists, Japan.

Bibliography

- [1] G. W. Frazer: X-ray Detectors in Astronomy (Cambridge University Press, Cambridge, 1989) p. 208.
- [2] H. Tsunemi, K. Yoshita, and S. Kitamoto, *Jpn J. Appl. Physic*, **36**, (1997) 2906.
- [3] K. Yoshita, H. Tsunemi, K. C. Gendreau, G. Pennington and M. W. Bautz, *IEEE Trans. Nucl. Sci.*, **45**, (1998) 915.
- [4] M. J. Pivovarovoff, S. Jones, M. Bautz, S. Kissel, G. Prigozhin, G. Ricker, H. Tsunemi and E. Miyata, *IEEE Trans. Nucl. Sci.*, **45**, (1998) 164.
- [5] K. O. Mason, G. Bignami, A. C. Brinkman, A. Peacock, *Advances in Space Research*, **16**, (1995) 41.
- [6] D. H. Lumb, H. Eggel, R. Laine, A. Peacock, *Proc. SPIE*, **2808**, (1996) 326.
- [7] A. D. Short, A. Keay, M. J. L. Turner, *Proc. SPIE*, **3445**, (1998) 13.
- [8] H. Tsunemi, J. Hiraga, K. Yoshita and S. Kitamoto, *Jpn J. Appl. Physic*, **37**, (1998) 2734.
- [9] J. Hiraga, H. Tsunemi, K. Yoshita, E. Miyata and M. Ohtani: *Jpn. J. Appl. Phys.*, **37** (1998) 4627.
- [10] H. Tsunemi, J. Hiraga, K. Yoshita and E. Miyata, *Jpn. J. Appl. Phys.*, **38** (1999) 2953.
- [11] H. Tsunemi, J. Hiraga, K. Yoshita, and K. Hayashida, *Nucl. Instr. and Meth*, **A421** (1999) 90.
- [12] H. Tsunemi, J. Hiraga, K. Mori, K. Yoshita and E. Miyata, *Nucl. Instr. and Meth*, (1999) in press.
- [13] K. Yoshita, H. Tsunemi, K. C. Gendreau, and M. W. Bautz, *IEEE trans. NS*, **46** (1999) 100.